The endocast morphology of LES1, Homo naledi

Shawn Hurst, Ralph Holloway, Antoine Balzeau, Heather Garvin, William Vanti, Lee Berger, John Hawks

The endocast morphology of LES1, *Homo naledi*

Shawn D. Hurst[1], Ralph L. Holloway[2], Antoine Balzeau[3,4], Heather M. Garvin[5,6], William B. Vanti[7], Lee R. Berger[6,8,9], and John Hawks[6,10].

[1]Department of Biology, University of Indianapolis, Indianapolis, United States.
[2]Department of Anthropology, Columbia University, New York, United States.
[3]Département Homme et Environnement, Muséum National d'Histoire Naturelle, PaleoFED team, Paris, France.
[4]Department of African Zoology, Royal Museum for Central Africa, B-3080 Tervuren, Belgium
[5]Department of Anatomy, Des Moines University, Des Moines, United States
[6]Centre for the Exploration of the Deep Human Journey, University of Witwatersrand, Johannesburg South Africa.
[7]Science and Engineering Library, Columbia University, New York, United States.
[8]The National Geographic Society, Washington DC, United States
[9]The Carnegie Institution for Science, Washington D.C., United States
[10]Department of Anthropology, University of Wisconsin-Madison, Madison, United States.

[*]Correspondence to: Shawn D. Hurst (hursts@uindy.edu)

Competing Interest Statement: The authors do not know of any competing interests.

Abstract

The evolutionary diversity across the genus *Homo* encompasses variation in brain size and overall brain shape. *Homo naledi*, from the Rising Star cave system of South Africa, is near the extreme of small brain size within *Homo* but is easily recognized as *Homo* in other aspects of endocast morphology. Previous work on the endocast of *H. naledi* has focused on cranial fossils from the Dinaledi Chamber. Here we add evidence of the endocast morphology of *Homo naledi* with the LES1 cranium from the Lesedi Chamber. This is the most complete representation of endocranial morphology yet known for *H. naledi* and confirms the anatomical form from more fragmentary material from the Dinaledi Chamber. Global endocast measurements show a posteriorly wide shape in *H. naledi* relative to endocranial volume. Qualitative description and metric comparisons show that LES1 and the DH3 endocast have derived morphology relative to chimpanzees and australopiths of the posterolateral frontal lobe and posterior occipital/parietal region. These traits are shared with *Homo sapiens* and endocasts of later *Homo erectus* and Neandertals. The orbital cap morphology may reflect a common ancestry of *H. naledi* with these groups, or parallelism between this smaller-brained lineage and species with larger brain sizes.

Keywords: Human evolution, brain, endocast, paleoneurology, *Homo naledi*

1. INTRODUCTION

Anthropologists long considered large brain size to be a defining feature of our genus (Leakey, Tobias, & Napier, 1964; Wood & Collard 1999; Garvin et al. 2017). Working with a less complete fossil record, researchers often interpreted the pattern of Pleistocene evolution of brain size as a gradual, geometric, or stepped increase over time, whether within a single evolving lineage (Lee & Wolpoff 2003) or across several taxa (Leigh 1992; Du et al. 2018). The discovery of Middle and Late Pleistocene species of *Homo* with absolutely and relatively small brain volumes, including *Homo naledi* and *Homo floresiensis*, has shown a greater diversity of brain size in extinct *Homo*. Analyses of endocasts have shown that despite their small brain sizes, *H. naledi* and *H. floresiensis* shared aspects of brain structure with *Homo sapiens* and some fossils of *Homo erectus* (Falk et al. 2005; Holloway et al., 2018). These findings suggested that brain structure, rather than brain size, may have been important to the initial evolution and diversification of *Homo* (Holloway et al., 2018).

However, recent work has questioned this hypothesis by suggesting that the samples of early *H. erectus* from Dmanisi and the Turkana Basin have apelike frontal lobe organizations, while later samples of *H. erectus* include significant heterogeneity in this anatomical region (Ponce de León et al. 2021). They do this by implying that the position of the superior precentral sulcus relative to the coronal suture is predictive of the position of the inferior precentral sulcus relative to the orbital cap. This prediction does not hold. The entirety of the precentral sulcus is visible on DH3 and the inferior precentral sulcus is found posterior to the orbital cap as is seen in *Homo sapiens* rather than crossing the orbital cap as is seen in *Pan* (see Fig. 3 and especially Fig. S5 in Holloway et al. 2018). Here we provide further evidence that changes in brain structure were independent of changes in brain size during the initial evolution of *Homo* using diverse species including *Homo naledi*.

We reconstructed and analyzed the endocast of the LES1 skeleton, from the Lesedi Chamber of the Rising Star cave system (Hawks et al. 2017). This skeleton is the most complete *H. naledi* individual yet described, with facial, mandibular, and vault morphology matching those of the Dinaledi Chamber sample (Hawks et al. 2017, Berger et al. 2015). We examined the original fossil material and high-resolution three-dimensional (3D) surface models of the LES1 cranial remains to reconstruct the preserved portions of its endocast. This more complete specimen enabled us to test the anatomical conclusions previously obtained from the fragmentary endocasts of *H. naledi* from the Dinaledi Chamber (Holloway et al., 2018). With this additional data, we carried out metric analyses to compare *H. naledi* with a broad sample of recent humans (*H. sapiens)*, chimpanzees (*P. troglodytes*), and fossil hominins. This work provides new quantitative data on the endocranial form of *H. naledi* in relation to fossil and extant hominins.

2. MATERIALS AND METHODS

The *Homo naledi* sample comprises DH1, DH3 and DH4 as well as LES1. The fossil hominin comparative sample includes *A. africanus* (Sts 5, Sts 71, Sts 60), *Paranthropus robustus* (SK1585), *Paranthropus boisei* (KNM-WT 13750, 17000, OH 5, OMO 338), *H. habilis sensu lato* (KNM-ER 1805, 1813, OH 13 and 16), *H. floresiensis* (LB1), *H. erectus sensu lato* (KNM-WT 15000, KNM-ER 3733, 3883, OH 9, OH 12, Sambungmacan 3, Ngandong 7, 12, Ngawi, Sangiran 2, Zhoukoudian 3, 10, 12), *H. heidelbergensis* (Bodo, Broken Hill), *H. neanderthalensis* (La Chapelle-aux-Saints, Guattari, Saccopastore 1, Feldhofer, Reilingen, Krapina 3, Spy 2, Abri Pataud, and Cro-Magnon 1). Fossil specimens were included in this comparative sample that include the same anatomical area preserved in LES1. In addition, we included data from 45 recent *H. sapiens*, 16 *P. paniscus,* and 15 *P. troglodytes* individuals (Balzeau & Gilissen 2010). All analyses were performed on endocast models obtained from surface scanning, CT, or microCT modalities as described in previous work (Holloway et al., 2018; Balzeau, Gilissen, Holloway, Prima, & Grimaud-Herve 2014; Balzeau & Gilissen 2010).

Fragments comprising the LES1 cranial vault were scanned at the University of the Witwatersrand on a Nikon Metrology XTH 225/320 microtomography (microCT) scanner. Surface models of the ectocranial and endocranial surfaces were obtained from LES1 using a NextEngine 3D Scanner after physical reconstruction of the vault. Model processing was completed in Geomagic Wrap, with model lighting and curvature maps used to assist in evaluating endocast features. We created several physical models including 3D prints of the virtual endocast, a Smooth-On Equinox silicone cast made by S.H. from the interior surface of a 3D print of the skull reconstruction, and a Denstply Aquisil LV silicone cast made by R.H. from the interior of a 3D print made by W.V. from the virtual skull reconstruction by H.G. Endocast images presented in this manuscript are derived from the microCT models; both the microCT, surface scan, and physical models were reviewed for all qualitative descriptions. Sulci determination was made independently by three of us (SH, RLH and AB), followed by group discussions. Those features presented in this paper are limited to those in which there was a consensus on the features we could reasonably observe. Agreement on features between observers is particularly important given the qualitative nature of sulci identification and the reliance on subtle imprints in interpreting brain morphology.

For metric analyses we selected anatomical landmarks that represent the preserved anatomical area of the *H. naledi* endocasts. Landmarks included the frontal pole (PF), the most lateral extension of the orbital cap (B; Balzeau et al. 2014), the temporal pole (TP), the point of maximal endocranial width (W), the temporo-cerebellar junction (TC), the point where the central sulci meet at their uppermost extension (C), the occipital pole (O), and endinion (E; Balzeau, Grimaud-Herve, & Gilissen 2011). Landmarks were positioned on each 3D model with Avizo 7 software by a single observer (AB) and then recollected three months later to assess interaobserver error. Intraobserver variation between those two trials was minimal (Figure S1), further confirmed by visual inspection.

We calculated all pairwise interlandmark distances, with mean, *N* and corrected coefficient of variation *V** for each taxon (Table S1, Supplementary File 1). *V** is a correction for small sample size bias in the estimate of CV, calculated as $(1 + 1/4N) \times CV$, where CV = SD/mean, both expressed in percentages (Sokal & Braumann 1980; Wood & Lieberman 2001). Measurements were examined both in absolute scale and relative to the cube root endocranial volume of each individual specimen. Statistical procedures were conducted with PAST 4.03 software (Hammer, Harper, & Ryan 2001).

In addition to these landmarks, we used the protocol and data from a previous study on the third frontal convolution (Balzeau et al. 2014) to compare the size and shape of this anatomical area in DH3 and LES1 of *H. naledi* with our comparative dataset (Balzeau et al. 2014; Mounier, Noûs, & Balzeau 2020). In this protocol, three anatomical points delimit the third frontal convolution, characterizing its antero-posterior extension and its lateral extension relative to this length. These points are: the center of the relief corresponding to the orbital part of the third frontal convolution, located on the relief between the lateral orbital sulcus anteriorly and the horizontal ramus of the lateral fissure posteriorly; the second point occurs in the maximal curvature of the triangular part of the third frontal convolution that characterizes the lateral extension and bulging of the orbital cap; the third point was the upper aspect of the Sylvian valley between the opercular part of the third frontal convolution and the temporal lobe.

We examined interlandmark distances with both univariate and multivariate methods. For each distance we compared groups using adjusted z-scores (Azs) (Scolan, Santos, Tillier, Maureille, & Quintard 2012), in which 95% of the variation of the reference population is included between –1 and +1. An Azs lower than –1 or higher than +1 is, therefore, outside 95% of the variation of the reference population. Our multivariate analyses included both principal component analyses (PCA) and linear discriminant analyses (LDA). Each of these was applied to absolute interlandmark distances and distances relative to the cube root endocranial volume of each specimen. In our LDA analyses we assigned most of our comparative sample to species groups, except for pooling *Australopithecus* and *Paranthropus*. Five fossil individuals were treated as unknowns with no *a priori* group assignments: the two *H. naledi* specimens (DH3 and LES1), the two *H. habilis* endocasts (KNM-ER 1813 and KNM-ER 1805) and LB1, holotype of *H. floresiensis*.

3. RESULTS

3.1 Preservation. The largest contiguous endocast surface of LES1 represents most of the left frontal, parietal, and temporal lobes, the superolateral aspect of the right frontal lobe, a portion of the left occipital lobe, a portion of the right parietal lobe, and the leftmost part of the cerebellum (Figure 1). Both left and right frontal poles are present on this preserved surface. Posteriorly, the preserved portion of the occipital bone does not extend to the midline. The endocranial surface is additionally represented on non-contiguous fragments of the right parietal, right temporal, and occipital. The cranial base of LES1 is not preserved, aside from a portion of the left lateral orbitofrontal, the basioccipital portion of the occipital bone, and fragments of left and right petrosals. On the contiguous endocast surface, there are four notable missing portions of 10-20 mm dimensions on the left endocast surface of the posterior frontal lobe, the temporal lobe, and the parietal lobe. Small cracks are visible across the reconstructed endocast surface representing junctions between cranial fragments. These cracks are mostly obvious interruptions of an otherwise smooth endocast surface. The bone fragments that constitute the vault exhibit no crushing, matrix expansion, or plastic distortion (Hawks et al. 2017, de Ruiter et al. 2019), and the preserved endocast surface appears to be free of any large-scale deformation. The external markings associated with the posterior portion of *M. temporalis* exhibit asymmetry

between the left and right temporal bones, possibly associated with pathology of the right suprameatal region (Hawks et al. 2017; de Ruiter et al. 2019) but we do not note any obvious signs of pathology on the endocast surface.

3.2 Qualitative description. More of the left orbital surface is present on LES1 than on any of the Dinaledi endocrania. The lateral part of the left middle orbital gyrus and the anterior part of the left posterior orbital gyrus as well as the entire left anterior and lateral orbital gyri are present. There is no evidence of a fronto-orbital sulcus incising the orbital margin. The frontal pole of the right hemisphere is slightly rostral in position to that of the left hemisphere, reflective of a right frontal petalia (Figures 1, S2-S3). The left lateral fissure with lateral (Sylvian) notch is present and ascending and horizontal rami of the lateral fissure are visible (Figure 1). The major frontal sulci incise the orbital margin at positions similar to modern human endocasts but grow fainter posteriorly (Figure 1). In contrast to the orbital surface, the dorsolateral surface of the anterior endocast has little detail. Portions of the precentral and central sulci are present (Figure 1).

The posterior endocast has little detail (Figures 1, S2). The sigmoid sinus is about 17.5 mm posterior to the foramen spinosum and middle meningeal artery. The sinus ends about 20 mm inferiorly. The upper part of the sigmoid sinus leads into a slightly elevated transverse sinus approximately 3 mm thick, and which terminates approximately 10 mm anterior to the mid-sagittal plane. The anatomy does not make clear whether the flow from the longitudinal sulcus was to the left or right side. The lateral part of the cerebellar lobe is rounded and full, and the greater horizontal cerebellar sulcus is visible extending from mid-sigmoid sinus to the inferior portion of the lateral sinus. Roughly 35 mm from the sigmoid sinus is the inferior portion of the remnant of the lambdoid suture, which is slightly visible for about 28 mm before ending in the broken portion of the parietal lobe. While very dim, it does appear in the expected area under the remnant, partially absorbed lambdoid suture seen on the ectocranium. Roughly 20 mm posterior to the lower limb of the suture is a faint groove, concave medially, which we believe is an outline of the left occipital pole, which is roughly 15 mm anterior to the mid-sagittal plane.

There is a deformity of the sigmoid sinus where it appears that the most inferior portion of the sigmoid sinus has been displaced medially. At the posterior extension of this inferior part of the sinus there is a hole on the endocranial surface that corresponds to the course of a diploic vein. A meningeal vein also continues posteriorly in this area in the continuation of the sinus. The sinus was possibly doubled, with the inferior one covering the sinus in the expected position, while the posterior extension has not been marked on the endocranial surface, possibly because it continued inside the brain. We regard the small crescentic groove as part of the occipital lobe just lateral to where the true occipital pole would be. There is no evidence for an inferior parietal sulcus on either side of the parietal lobe.

3.3 Metric analyses. Our metric analyses add new information about the *H. naledi* endocasts in comparison with the broader sample of fossil and recent material. The most interesting findings concern the quantitative assessment of the third frontal convolution. This anatomical area is well defined on both DH3 and LES1. Across all samples, variation (*V**) is similar in extent for the measurements of this region (Table 1). However, the absolute and relative dimensions for this anatomical area are different among hominid groups. Despite their small endocranial volumes, the two *H. naledi* specimens, DH3 and LES1, each have absolute third frontal convolution measures that enter the upper half of the variation for *H. sapiens*, *H. erectus*, and *H. neanderthalensis*. When examined relative to the cube root of endocranial volume, *H. naledi* ranks among the highest values in these samples of *Homo*. Both absolute and relative values for the *H. naledi* specimens are far above *Pan*, *Australopithecus,* and *Paranthropus* (Balzeau et al. 2014).

Global interlandmark distances reflect the small size of LES1 and other *H. naledi* endocasts. Absolute measures of *H. naledi* overlap the range of variation of *Au. africanus*, *Paranthropus*, and *H. habilis* (Table S1). These absolute measures tend to be significantly smaller than *H. sapiens* and larger than *Pan* (Table S3). When interlandmark distances are considered relative to cube root endocranial volume (Table S2), *H. naledi* endocasts are relatively larger than both *H. sapiens* and *Pan* for distances from frontal pole to the endocast's maximum width and the frontal pole to the temporo-cerebellar junction (Table S4). Both these measures suggest a wide endocast relative to volume, particularly posteriorly (Table S1, S2, Supplementary File 1).

The first two components of the principal component analysis (PCA) computed on the absolute interlandmark distances represent respectively 86.4% and 5.9% of the total variance (Figures S4-S5). Loadings of all the variables are positive in PC1 which is strongly related to endocranial volume; PC2 encompasses mostly within-species variation seen across the broad sample. To explore the extent of shape differentiation of groups, we conducted linear discriminant analysis (LDA) on the same absolute data (Figures 2, S6). LDA provided good separation of groups with similar brain sizes and did separate the *H. naledi* endocasts from *H. habilis* and *Australopithecus*, but size was the largest contributor to group separation. To examine variation in shape relative to endocranial size, we computed a relative LDA with interlandmark distances scaled to cube root endocranial volume (Figure S7). This analysis also produced good separation of *H. sapiens*, *Pan*, *Australopithecus-Paranthropus* and *H. erectus*, while Neandertals overlap with *H. sapiens* and *H. erectus*. This analysis separated the two *H. habilis* endocasts from both *Australopithecus-Paranthropus* and *Pan*. As in the absolute LDA, LB1 of *H. floresiensis* clusters with *Pan*. LES1 plots in an area of extensive overlap between species, near Abri Pataud (*H. sapiens*), Bodo (Middle Pleistocene human), Ngandong 7 (*H. erectus*) and one *P. paniscus* individual, although this relative LDA does distinguish it clearly from *Australopithecus* and *Paranthropus*.

In sum, *H. naledi* generally resembles other hominins with small brain size in absolute measurements. Where it is more distinctive is in its low but posteriorly located maximal width and long distance to the junction of the frontal and parietal lobes, particularly when scaled by cube root endocranial volume. The *H. naledi* endocasts contrast metrically from other hominins with small brain size in the orbital cap, which is comparable in absolute and relative size to species of *Homo* with much larger brain sizes. This portion of the LES1 endocast is similar to that in the smaller DH3, and the variation between these two is comparable to variation observed in other species of hominins.

4. DISCUSSION

The anatomy of LES1 confirms the size and form of the orbital cap in *H. naledi*. Some have suggested that the morphology of the orbital cap is not reliably assessed in an endocast (Ponce de León et al. 2021). The discovery of LES1 enabled us to test this assertion for *H. naledi* with a new endocast not included in our previous examinations from the Dinaledi Chamber. Both qualitative and quantitative analyses show consistency between LES1 and other *H. naledi* endocasts, show that *H. naledi* had a level of variation in this region comparable to that seen in extant species, and confirm the shared morphology of *H. naledi* with *H. sapiens*, Neandertals, and some specimens of *H. erectus*. This shared morphology across lineages that otherwise differ in size and global endocast shape suggests that this frontal lobe morphology retained adaptive value across lineages with varied ecologies, body sizes, and life histories. It has been suggested that the functions of this brain area in communication (Balzeau et al. 2014; Schoenemann & Holloway 2016), social and emotional cognition (Kringelbach & Rolls 2004), and possibly tool manufacture (Stout, Toth, Schick, & Chaminade 2008; Putt, Wijeakumar, Franciscus, & Spencer 2017) may have been important to the origin and evolution of *Homo.*

A broad array of work shows that different lineages within *Homo* exhibited diverse evolutionary patterns in endocast shape and size. The early evolution of *H. sapiens* involved shape changes to the endocast, but little increase in brain size (Hublin et al. 2017). The evolution of *H. neanderthalensis* from earlier to later samples involved endocast shape changes together with an increase in endocranial volume (Poza-Rey, Gomez-Robles, & Arsuaga 2019). *Homo erectus* increased in brain size across its long existence, and comparisons of endocast shape between early African and later Asian samples of *H. erectus s.l.* (sometimes distinguished as two species, *H. ergaster* and *H. erectus*) show contrasts between these regional samples (Pearson, Polly, & Bruner 2021).

With this growing evidence of evolutionary diversity in brain shape across *Homo*, lineages with smaller brain sizes, like *H. naledi*, *H. habilis*, and *H. floresiensis*, are of great interest. At present, only a handful of endocasts representing these lineages are complete enough to consider global aspects of endocast shape. It is not clear whether *H. floresiensis*, *H. naledi*, or both may have evolved from ancestors with larger brain size.

The endocast shape of LB1 (*H. floresiensis*), while sharing some aspects of endocast shape with *H. erectus*, occupies a very distinctive place in shape space compared to either *H. erectus* or other hominins (Falk et al. 2005); although some have suggested that pathology may play a role in the morphology of this individual (Holloway 2010). Neubauer and colleagues (Neubauer, Hublin, & Gunz 2018) included KNM-ER 1813 (*H. habilis*) and KNM-ER 1470 (*H. rudolfensis*) in a morphometric analysis of endocranial shape in *H. erectus*, finding that these two endocasts each are distinct from *H. erectus* and *H. sapiens* in different shape dimensions. In our present study, we find that the lateral and posterior cranial shape of *H. naledi* sets it apart from *H. habilis* although the two species overlap in size.

The LES1 endocast adds to the evidence that *H. naledi* had a relatively and absolutely large orbital cap with morphology similar to *Homo* species that have larger brain sizes (Holloway et al., 2018). The current study of *H. naledi* material does not address whether this morphology is shared with early fossils of *H. erectus* including the Dmanisi sample, which have been suggested to differ from later *H. erectus* and *H. sapiens* based on the position of the superior precentral sulcus relative to the coronal suture (Ponce de León et al. 2021); however this condition does not appear to be predictive of orbital cap morphology (Holloway et al. 2018). Previous work suggested that some early African and Indonesian representatives of *H. erectus* had smaller orbital cap areas than later *H. erectus* (Balzeau et al. 2014), and the current study places *H. naledi* among the larger *H. erectus* and *Homo sapiens* samples—in contrast to *H. floresiensis* and *H. habilis* endocasts. It is possible that this morphology links *H. naledi* with later *H. erectus* and *H. sapiens*, consistent with the hypothesis that these may share a common ancestor in the later Early Pleistocene (Dembo et al. 2016). Alternatively, orbital cap morphology may exhibit significant parallelism between these lineages. Testing these alternatives would benefit from closer morphological assessment of this region in hominins that have been underrepresented in studies of complete endocasts.

AUTHOR CONTRIBUTIONS:

SH performed research, analyzed data, presented the research at conference, helped write the paper, and did manuscript editing. RH did fossil reconstruction, performed research, analyzed data, and did manuscript editing; AB designed research, performed research, analyzed data, helped write the paper, and did manuscript editing; HM created 3D scans, did fossil reconstruction, analyzed data, and did manuscript editing; WV generated 3D prints of endocasts; LB designed research, led excavation and research, created 3D scans, analyzed data, and did manuscript editing; JH designed research, led excavation and research, analyzed data, helped write the paper, and did manuscript editing.

Acknowledgments

3D surface data of the *H. naledi* fossil material in this analysis is available from Morphosource.org. This work was supported by the National Geographic Society, the National Research Foundation of South Africa, the Lyda Hill Foundation, the Fulbright Scholar Program, the Centre of Excellence in PalaeoSciences, South Africa, the Vilas Trust, and the Wisconsin Alumni Research Foundation.

REFERENCES

Balzeau, A., & Gilissen, E. (2010). Endocranial shape asymmetries in *Pan paniscus*, *Pan troglodytes* and *Gorilla gorilla* assessed via skull based landmark analysis. *Journal of Human Evolution*, *59*, 54-69.

Balzeau, A., Gilissen, E., Holloway, R. L., Prima, S., & Grimaud-Herve, D. (2014). Variations in size, shape and asymmetries of the third frontal convolution in hominids: Paleoneurological implications for hominin evolution and the origin of language. *Journal of Human Evolution*, *76*, 116-128.

Balzeau, A., Grimaud-Herve, D., & Gilissen, E. (2011). Where are inion and endinion? Variations of the exo- and endocranial morphology of the occipital bone during hominin evolution. *Journal of Human Evolution*, *61*, 488-502

Berger, R.L., Hawks, J., de Ruiter, D.J., Churchill, S.E., Schmid, P., Delezene, L.K., Kivell, T.L., Garvin, H.M., Williams, S.A., DeSilva, J.M., Skinner, M.M., Musiba, C.M., Cameron, N., Holliday, T.W., Harcourt-Smith, W., Ackermann, R.R., Bastir, M., Bogin, B., Bolter, D., Brophy, J., Cofran, Z.D., Congdon,

K.A., Deane, A.S., Dembo, M., Drapeau, M., Elliott, M.C., Feuerriegel, E.M., Garcia-Martinez, D., Green, D.J., Gurtov, A., Irish, J.D., Kruger, A., Laird, M.F., Marchi, D., Meyer, M.R., Nalla, S., Negash, E.W., Orr, C.M., Radovcic, D., Schroeder, L., Scott, J.E., Throckmorton, Z., Tocheri, M.W., VanSickle, C., Walker, C.S., Wei, P., & Zipfel, B. (2015). *Homo naledi*, a new species of the genus *Homo* from the Dinaledi Chamber, South Africa. *Elife*, *4*, Article e09560.

Dembo, M., Radovcic, D., Garvin, H. M., Laird, M. E., Schroeder, L., Scott, J. E., Brophy, J., Ackermann, R. R., Musiba, C. M., de Ruiter, D. J., Mooers, A. O., & Collard, M. (2016). The evolutionary relationships and age of *Homo naledi*: An assessment using dated Bayesian phylogenetic methods. *Journal of Human Evolution*, *97*, 17-26.

Du, A., Zipkin, A. M., Hatala, K. G., Renner, E., Baker, J. L., Bianchi, S., Bernal, K. H., & Wood, B. A. (2018). Pattern and process in hominin brain size evolution are scale-dependent. *Proceedings of the Royal Society B-Biological Sciences*, *285*, Article 20172738.

Falk, D., Hildebolt, C., Smith, K., Morwood, M. J., Sutikna, T., Brown, P., Jatmiko, Saptomo, E. W., Brunsden, B., & Prior, F. (2005). The brain of LB1, *Homo floresiensis*. *Science*, *308*, 242-245.

Garvin, H. M., Elliott, M. C., Delezene, L. K., Hawks, J., Churchill, S. E., Berger, L. R., & Holliday, T. W. (2017). Body size, brain size, and sexual dimorphism in *Homo naledi* from the Dinaledi Chamber. *Journal of Human Evolution*, *111*, 119-138.

Hammer, Ø., Harper, D. A., & Ryan, P. D. (2001) PAST: Paleontological statistics software package for education and data analysis. *Palaeontologia Electronica* 4, 9.

Hawks, J., Elliott, M., Schmid, P., Churchill, S. E., de Ruiter, D. J., Roberts, E. M., Hilbert-Wolf, H., Garvin, H. M., Williams, S. A., Delezene, L. K., Feuerriegel, E. M., Randolph-Quinney, P., Kivell, T. L., Laird, M. F., Tawane, G. DeSilva, J. M., Bailey, S. E., Brophy, J. K., Meyer, M. R., Skinner, M. M., Tocheri, M. W., VanSickle, C., Walker, C. S., Campbell, T. L., Kuhn, B., Kruger, A., Tucker, S. Gurtov, A., Hlophe, N., Hunter, R., Morris, H., Peixotto, B., Ramalepa, M., van Rooyen, D., Tsiloane, M., Boshoff, P., Dirks, P. H. G. M., & Berger, L. R. (2017) New fossil remains of *Homo naledi* from the Lesedi Chamber, South Africa. *Elife* 6, e24232.

Holloway, R. (2010) Human brain endocasts, Taung, and the LB1 Hobbit brain. In D. Broadfield, M. Yuan, K. Schick, and N. Toth (Eds.) *The human brain evolving: paleoneurological studies in honor of Ralph L. Holloway*. Gosport: Stone Age Institute.

Holloway, R. L., Hurst, S. D., Garvin, H. M., Schoenemann, P. T., Vanti, W. B., Berger, L. R., & Hawks, J. (2018). Endocast morphology of *Homo naledi* from the Dinaledi Chamber, South Africa. *Proceedings of the National Academy of Sciences of the United States of America* 115, 5738-5743.

Hublin, J. J., Ben-Ncer, A., Bailey, S. E., Freidline, S. E., Neubauer, S., Skinner, M. M., Bergmann, I., Le Cabec, A., Benazzi, S., Harvati, K., & Gunz, P. (2017) New fossils from Jebel Irhoud, Morocco and the pan-African origin of *Homo sapiens*. Nature 546, 289-292.

Kringelbach, M., & Rolls, E., (2004) The functional neuroanatomy of the human orbitofrontal cortex: evidence from neuroimaging and neuropsychology. *Progress in Neurobiology* 72, 341-372.

Leakey, L. S. B., Tobias, P. V., & Napier, J. R. (1964) A New Species of The Genus *Homo* From Olduvai Gorge. *Nature* 202, 7-9.

Lee, S., & Wolpoff, M. (2003) The pattern of evolution in Pleistocene human brain size. *Paleobiology*, 29, 186-196.

Leigh, S. R. (1992) Cranial capacity evolution in *Homo erectus* and early *Homo sapiens*. *American Journal of Physical Anthropology* 87, 1-13.

Mounier, A., Noûs, C., & Balzeau, A. (2020) Palaeoneurology and the emergence of language. *Bulletins et Mémoires de la Société d'Anthropologie de Paris* 32, 147-157.

Neubauer, S., Hublin, J.-J., & Gunz, P. (2018) The evolution of modern human brain shape. *Science Advances* 4, eaao5961.

Pearson, A., Polly, P. D., & Bruner, E. (2021). Temporal lobe evolution in Javanese *Homo erectus* and *African*
Homo ergaster: inferences from the cranial base. *Quaternary International*, *603*, 5-21.

Ponce de León M. S., Bienvenu, T., Marom, A., Engel, S., Tafforeau, P., Alatorre Warren, J. L., Lordkipanidze, D., Kurniawan, I., Murti, D. B., Suriyanto, R. A., Koesbardiati, T., Zollikofer, C. P. E. (2021) The primitive brain of early *Homo*. *Science* 372, 165-171.

Poza-Rey, E. M., Gomez-Robles, A., & Arsuaga, J. L. (2019) Brain size and organization in the Middle Pleistocene hominins from Sima de los Huesos. Inferences from endocranial variation. *Journal of Human Evolution* 129, 67-90.

Putt, S. S., Wijeakumar, S., Franciscus, R. G., & Spencer, J. P. (2017) The functional brain networks that underlie Early Stone Age tool manufacture. *Nature Human Behaviour* 1, 1-8.

de Ruiter, D. J., Laird, M. F., Elliott, M., Schmid, P., Brophy, J., Hawks, J., & Berger, L. R. (2019). *Homo naledi* cranial remains from the Lesedi chamber of the rising star cave system, South Africa. *Journal of Human Evolution*, 132, 1-14.

Schoenemann, P. T., & Holloway R. L. (2016) Brain function and Broca's Cap: A meta-analysis of fMRI studies. *American Journal of Physical Anthropology* 159, 283-283

Scolan, H., Santos, F., Tillier, A. M., Maureille, B., & Quintard, A. (2012) Des nouveaux vestiges néanderthaliens à Las Pélénos (Monsempron-Libos, Lot-et-Garonne, France). *Bulletins et Mémoires de la Société d'Anthropologie de Paris 24, 69-95.*

Sokal, R. R., & Braumann, C. A. (1980) Significance tests for coefficients of variation and variability profiles. *Systematic Biology* 29, 50-66.

Stout, D., Toth, N., Schick, K., & Chaminade, T. (2008) Neural correlates of Early Stone Age toolmaking: technology, language and cognition in human evolution. *Philosophical Transactions of the Royal Society B: Biological Sciences* 363, 1939-1949.

Wood, B., & Collard, M. (1999) The human genus. *Science* 284, 65-71.

Wood, B., & Lieberman, D. E., (2001) Craniodental variation in *Paranthropus boisei*: a developmental and functional perspective. *American Journal of Physical Anthropology 116, 13-25.*

Figure and Table Legends

Figure 1.
LES1 (*Homo naledi)* virtual endocast illustrated in (A) left lateral; (B) superior; and (C) rostral views. Ideograms of the cranial vault illustrate each angle. (D) Left lateral view with sulci and fissures drawn for illustration: 1. Superior frontal sulcus; 2. middle frontal sulcus; 3. inferior frontal sulcus; 4. ascending ramus of the lateral fissure; 5. horizontal branch; 6. precentral sulcus; 7. central sulcus; 8. lateral fissure; 9. transverse fissure; 10. inferior portion of sigmoid sinus. (E) Oblique detail view of the LES1 left orbital cap, unlabeled (left) and labeled (right) 1. Horizontal branch; 2. ascending ramus of the lateral fissure.

Figure 2.
Results of linear discriminant analyses (LDA). (A) LDA based on absolute interlandmark distances. In this analysis, axis 1 is strongly correlated with endocranial volume, while axis 2 correlates with endocast height relative to length, attaining separation of modern and Neandertal crania (left) and H. naledi from H. habilis and Australopithecus-Paranthropus (right). (B) LDA based on interlandmark distances relative to cube root endocranial volume. In these results, H. naledi is not clearly separated from H. erectus or P. paniscus, and LES1 falls in an area of extensive overlap of H. sapiens, H. erectus, and P. paniscus. Individuals near LES1 in this comparison are Abri Pataud (H. sapiens), Ngandong 7 (H. erectus), Bodo (Middle Pleistocene human) and two P. paniscus individuals.

Figure 3.
Bivariate plot of the size of the third frontal convolution (square root, noted 3Fc, in mm) and of the endocranial volume (cube root, noted Endo V, in mm) in Pan paniscus (triangles), Pan troglodytes (inverted triangles), H. sapiens (circles), fossil H. sapiens (black circles), fossil hominins (black diamonds: T: Taung, 17k: KNM-WT 17000, 1470: KNM-ER 1470, 1813: KNM-ER 1813, 3733: KNMER 3733, 3883: KNM-ER 3883, 15k: KNM-WT 15000, OH 9, D: Dmanisi 9002, T2: Trinil 2, S2: Sangiran 2, S17: Sangiran 17, M: Mojokerto, Ng7: Ngandong 7, Ng12: Ngandong 12, Sm3: Sambungmacan 3, S3: Zhoukoudian Ckn. E 1.PA.16, S12: Zhoukoudian Ckn. L 2.PA.100, LB 1: Liang Bua 1, SV: Skhūl V, Ar: Arago, B: Bodo, K: Kabwe 1, JB1: Jebel Irhoud 1, P: Petralona, S: Salé) and Neandertals (red circle, F: Feldhofer, LC: La Chapelle-aux-Saints 1, LF1: La Ferrassie 1, Gu: Guattari, Gi: Gibraltar, K3: Krapina 3, Q5: La Quina H5, Sa: Saccopastore, TC1: Tabun C1, TT: Teshik Tash, SII: Spy 10 modified from Mounier and al., 2020). The green circle refers to the two analysed Homo naledi specimens.

Table 1.
Measurements of the third frontal convolution (mean values for HF3: height of the 3rd frontal convolution, LF3: length of the 3rd frontal convolution both are in mm, SF3: surface of the 3rd frontal convolution in mm^2, HF3r and LF3r are dimensions for HF3 and LF3 relative to cube root endocranial volume; *N*: number of individuals *V**: coefficient of variation corrected for small samples) in the different analyzed samples. See also Supplemental File 1.

Supplementary Figure S1.
Landmarks used in metric analyses. PF= Frontal pole; B= most lateral extension of the orbital (Broca's) cap; TP= Temporal pole, W=Point of maximal endocranial width; TC= Temporo-cerebellar junction, C= Point where the central sulci meet at their uppermost extension; O= Occipital pole; E= Endinion.

Supplementary Figure S2.
Preservation of LES1 endocast compared to individuals from the Dinaledi Chamber. LES1 (top left) preserves nearly all the left side of the endocast except for the extremely posterior portion of the occipital lobe and cerebellum. It also preserves some portions of the right parietal lobe and most of the right frontal lobe contiguous with the left side. DH3 (top right) preserves left frontal, left temporal, and left parietal portions with a portion of the left cerebellum but none of the right

side. DH1 (middle right) preserves the posterior endocranial surface and portions of both parietal lobes on two different preserved portions of the cranium. DH2 (middle left, shown here reversed) preserves portions of both parietal lobes, right temporal, and right occipital portions. DH4 (bottom left, shown here reversed) preserves portions of right cerebellar, occipital, temporal, and parietal lobes. DH3 has the best gyral and sulcal detail, with LES1 approaching this level of detail in selected portions.

Supplementary Figure S3.
LES1 silicone endocast physical model in left lateral (top) and basal (bottom) views. This model uses comparative data to build the basicranial anatomy. The measured volume of this reconstruction is 590cc, smaller than the digital reconstruction which had a volume of 610cc (Holloway et al., 2018). 1, Meningeal vessel; 2, lambdoid suture; 3, small sulcus of occipital lobe and pole; 4, sigmoid sinus; 5, interior portion of sigmoid sinus, displaced; 6, greater cerebellar horizontal sulcus.

Supplementary Figure S4.
Results of principal components analysis (PCA) based on interlandmark distances. PC1 accounts for 86.4% of the variance and has positive weights on all underlying interlandmark distances. The rank order of fossil hominins on this axis is basically in order of endocranial volume. PC2 accounts for 5.9% of the variance and appears to show a degree of within-group variation in each sample.

Supplementary Figure S5.
Results of principal components analysis (PCA) based on interlandmark distances relative to cube root endocranial volume. In this analysis, PC1 still appears correlated with endocranial size, although with length relative to height reflected in this dimension.

Supplementary Figure S6.
Results of linear discriminant analysis (LDA) based on absolute interlandmark distances. These results are also reported in main text Figure 2, here provided with all fossil hominin individuals labeled. Axis 1 is strongly correlated with endocranial volume, while axis 2 separates samples based on dimensions associated with endocast length relative to height. *H. naledi* in this analysis is well discriminated from other samples of similar endocranial volume, including *H. habilis*, *Australopithecus-Paranthropus*, and *H. erectus*.

Supplementary Figure S7.
Results of linear discriminant analysis (LDA) based on interlandmark distances relative to cube root endocranial volume. These results are also reported in main text Figure 2, here provided with all fossil hominin individuals labeled.

Table S1.
Data for endocranial measurements between pairs of points (mean value in mm, N: number of individuals, V*: coefficient of variation corrected for small samples) in the different analyzed samples. PF= frontal pole; B= most lateral extension of the orbital (Broca's) cap; TP= Temporal pole, W=Point of maximal endocranial width; TC= Temporo-cerebellar junction, C= Point where the central sulci meet at their uppermost extension; O= Occipital pole; E= Endinion. See also Supplemental Excel file.

Table S2.
Data for *relative* endocranial measurements between pairs of points (N: number of individuals, V*: coefficient of variation corrected for small samples) in the different analyzed samples. PF= frontal pole; B= most lateral extension of the orbital (Broca's) cap; TP= Temporal pole, W=Point of maximal endocranial width; TC= Temporo-cerebellar junction, C= Point where the central sulci meet at their uppermost extension; O= Occipital pole; E= Endinion. See also Supplemental Excel file. "*r*" indicates these are relative measurements. See also

Supplemental Excel file.

Table S3.
Data for endocranial measurements between pairs of points (mean value in mm) individual values for the different H. naledi fossils and Azs scores relative to the comparative samples. PF= frontal pole; B= most lateral extension of the orbital (Broca's) cap; TP= Temporal pole, W=Point of maximal endocranial width; TC= Temporo-cerebellar junction, C= Point where the central sulci meet at their uppermost extension; O= Occipital pole; E= Endinion. See also Supplemental Excel file.

Table S4.
Data for relative endocranial measurements between pairs of points individual values for the different H. naledi fossils and Azs scores relative to the comparative samples. PF= frontal pole; B= most lateral extension of the orbital (Broca's) cap; TP= Temporal pole, W=Point of maximal endocranial width; TC= Temporo-cerebellar junction, C= Point where the central sulci meet at their uppermost extension; O= Occipital pole; E= Endinion. See also Supplemental Excel file.

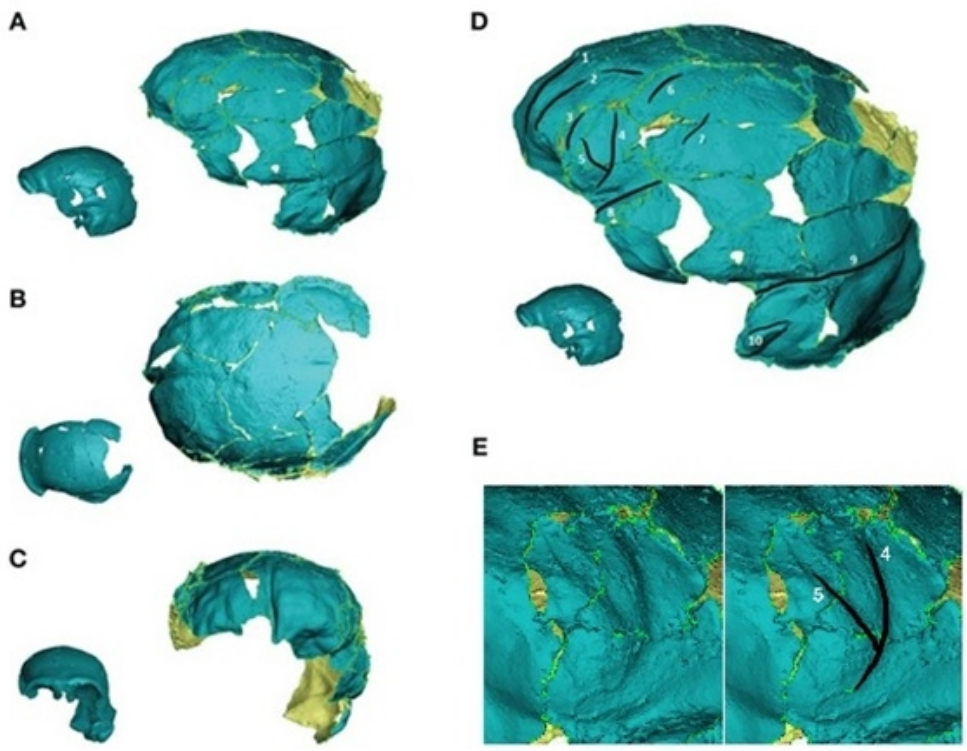

Figure 1.
LES1 (Homo naledi) virtual endocast illustrated in (A) left lateral; (B) superior; and (C) rostral views. Ideograms of the cranial vault illustrate each angle. (D) Left lateral view with sulci and fissures drawn for illustration: 1. Superior frontal sulcus; 2. middle frontal sulcus; 3. inferior frontal sulcus; 4. ascending ramus of the lateral fissure; 5. horizontal branch; 6. precentral sulcus; 7. central sulcus; 8. lateral fissure; 9. transverse fissure; 10. inferior portion of sigmoid sinus. (E) Oblique detail view of the LES1 left orbital cap, unlabeled (left) and labeled (right) 1. Horizontal branch; 2. ascending ramus of the lateral fissure.

152x118mm (96 x 96 DPI)

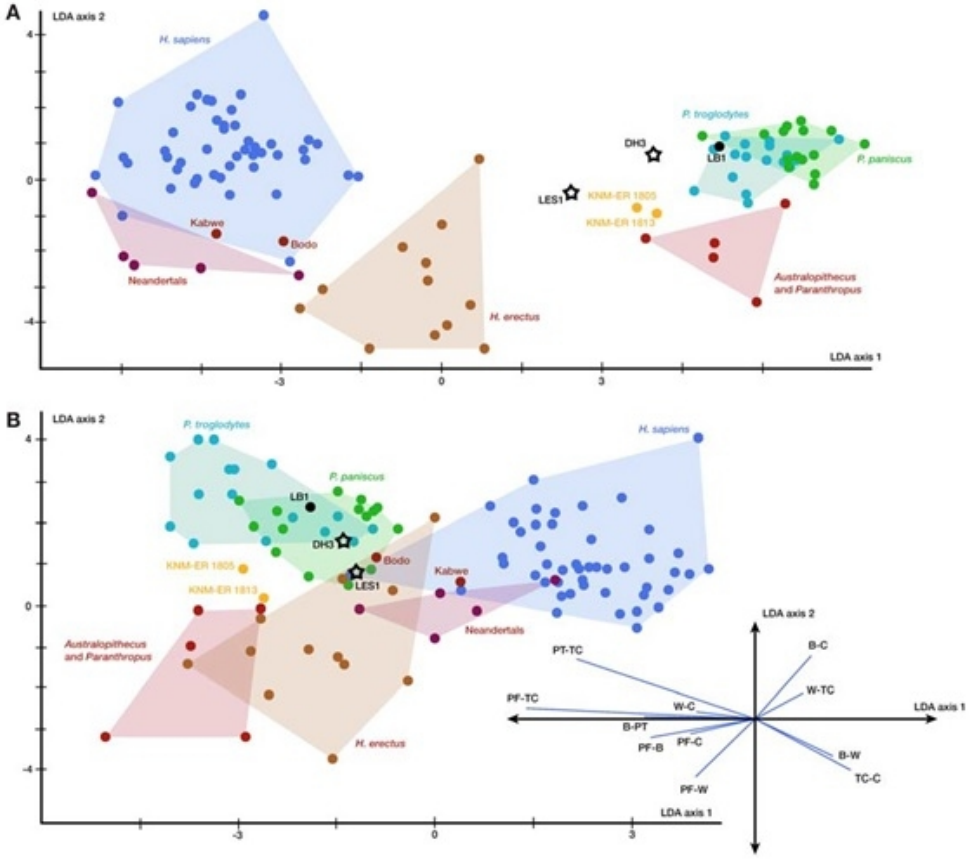

Figure 2.
Results of linear discriminant analyses (LDA). (A) LDA based on absolute interlandmark distances. In this analysis, axis 1 is strongly correlated with endocranial volume, while axis 2 correlates with endocast height relative to length, attaining separation of modern and Neandertal crania (left) and H. naledi from H. habilis and Australopithecus-Paranthropus (right). (B) LDA based on interlandmark distances relative to cube root endocranial volume. In these results, H. naledi is not clearly separated from H. erectus or P. paniscus, and LES1 falls in an area of extensive overlap of H. sapiens, H. erectus, and P. paniscus. Individuals near LES1 in this comparison are Abri Pataud (H. sapiens), Ngandong 7 (H. erectus), Bodo (Middle Pleistocene human) and two P. paniscus individuals.

152x142mm (96 x 96 DPI)

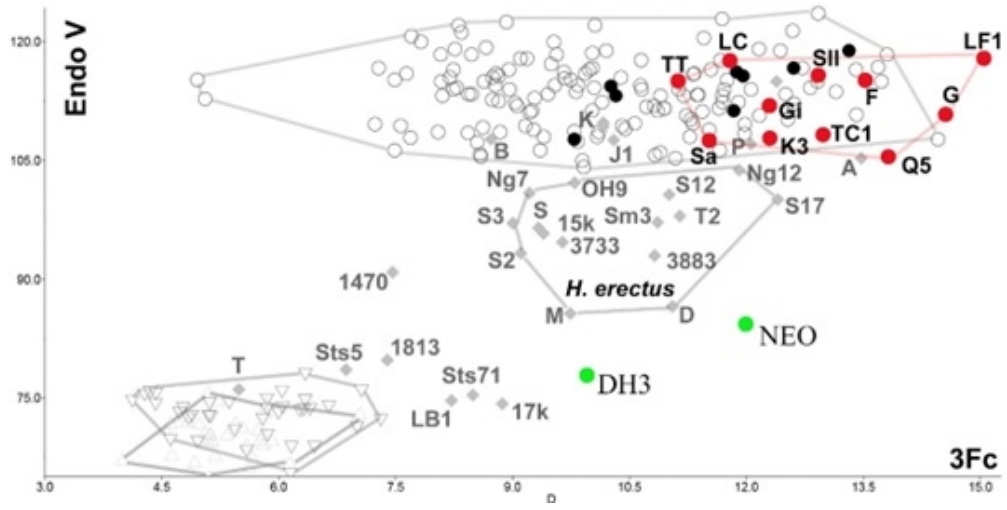

Figure 3.
Bivariate plot of the size of the third frontal convolution (square root, noted 3Fc, in mm) and of the endocranial volume (cube root, noted Endo V, in mm) in Pan paniscus (triangles), Pan troglodytes (inverted triangles), H. sapiens (circles), fossil H. sapiens (black circles), fossil hominins (black diamonds: T: Taung, 17k: KNM-WT 17000, 1470: KNM-ER 1470, 1813: KNM-ER 1813, 3733: KNMER 3733, 3883: KNM-ER 3883, 15k: KNM-WT 15000, OH 9, D: Dmanisi 9002, T2: Trinil 2, S2: Sangiran 2, S17: Sangiran 17, M: Mojokerto, Ng7: Ngandong 7, Ng12: Ngandong 12, Sm3: Sambungmacan 3, S3: Zhoukoudian Ckn. E 1.PA.16, S12: Zhoukoudian Ckn. L 2.PA.100, LB 1: Liang Bua 1, SV: Skhūl V, Ar: Arago, B: Bodo, K: Kabwe 1, JB1: Jebel Irhoud 1, P: Petralona, S: Salé) and Neandertals (red circle, F: Feldhofer, LC: La Chapelle-aux-Saints 1, LF1: La Ferrassie 1, Gu: Guattari, Gi: Gibraltar, K3: Krapina 3, Q5: La Quina H5, Sa: Saccopastore, TC1: Tabun C1, TT: Teshik Tash, SII: Spy 10 modified from Mounier and al., 2020). The green circle refers to the two analysed Homo naledi specimens.

142x71mm (96 x 96 DPI)

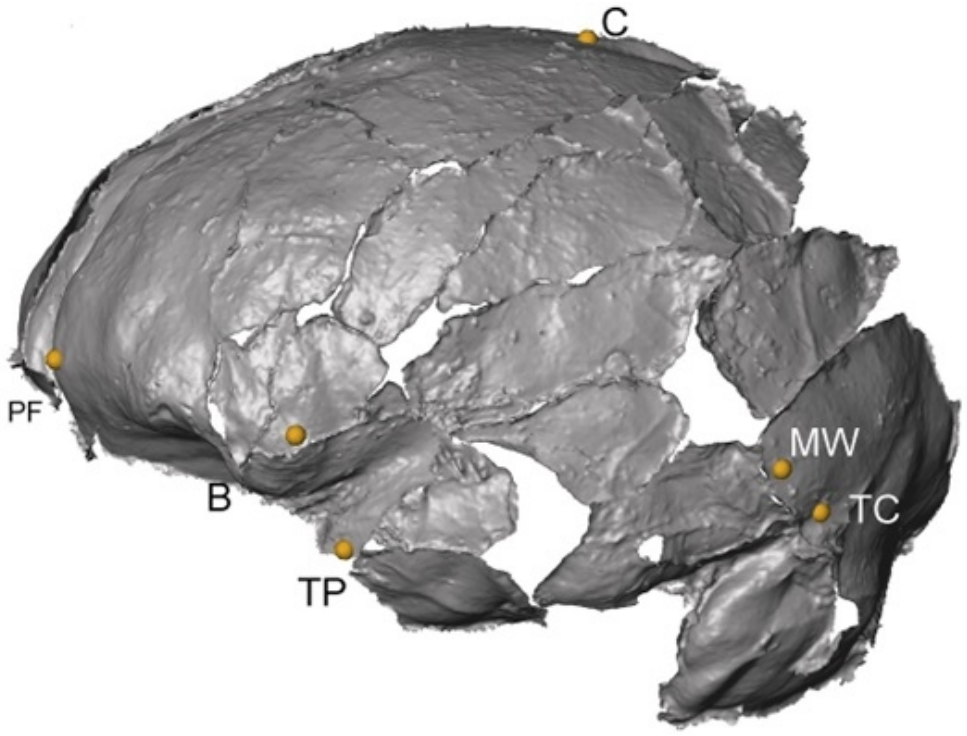

Supplementary Figure S1.
Landmarks used in metric analyses. PF= Frontal pole; B= most lateral extension of the orbital (Broca's) cap; TP= Temporal pole, W=Point of maximal endocranial width; TC= Temporo-cerebellar junction, C= Point where the central sulci meet at their uppermost extension; O= Occipital pole; E= Endinion.

142x104mm (96 x 96 DPI)

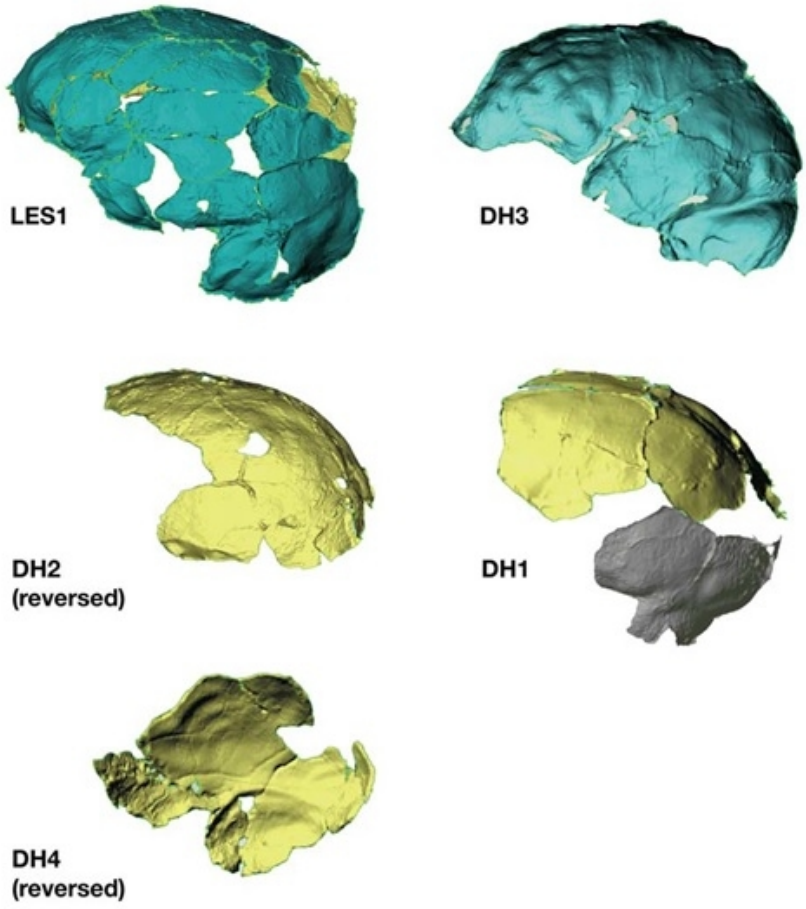

Supplementary Figure S2.
Preservation of LES1 endocast compared to individuals from the Dinaledi Chamber. LES1 (top left) preserves nearly all the left side of the endocast except for the extremely posterior portion of the occipital lobe and cerebellum. It also preserves some portions of the right parietal lobe and most of the right frontal lobe contiguous with the left side. DH3 (top right) preserves left frontal, left temporal, and left parietal portions with a portion of the left cerebellum but none of the right side. DH1 (middle right) preserves the posterior endocranial surface and portions of both parietal lobes on two different preserved portions of the cranium. DH2 (middle left, shown here reversed) preserves portions of both parietal lobes, right temporal, and right occipital portions. DH4 (bottom left, shown here reversed) preserves portions of right cerebellar, occipital, temporal, and parietal lobes. DH3 has the best gyral and sulcal detail, with LES1 approaching this level of detail in selected portions.

152x152mm (96 x 96 DPI)

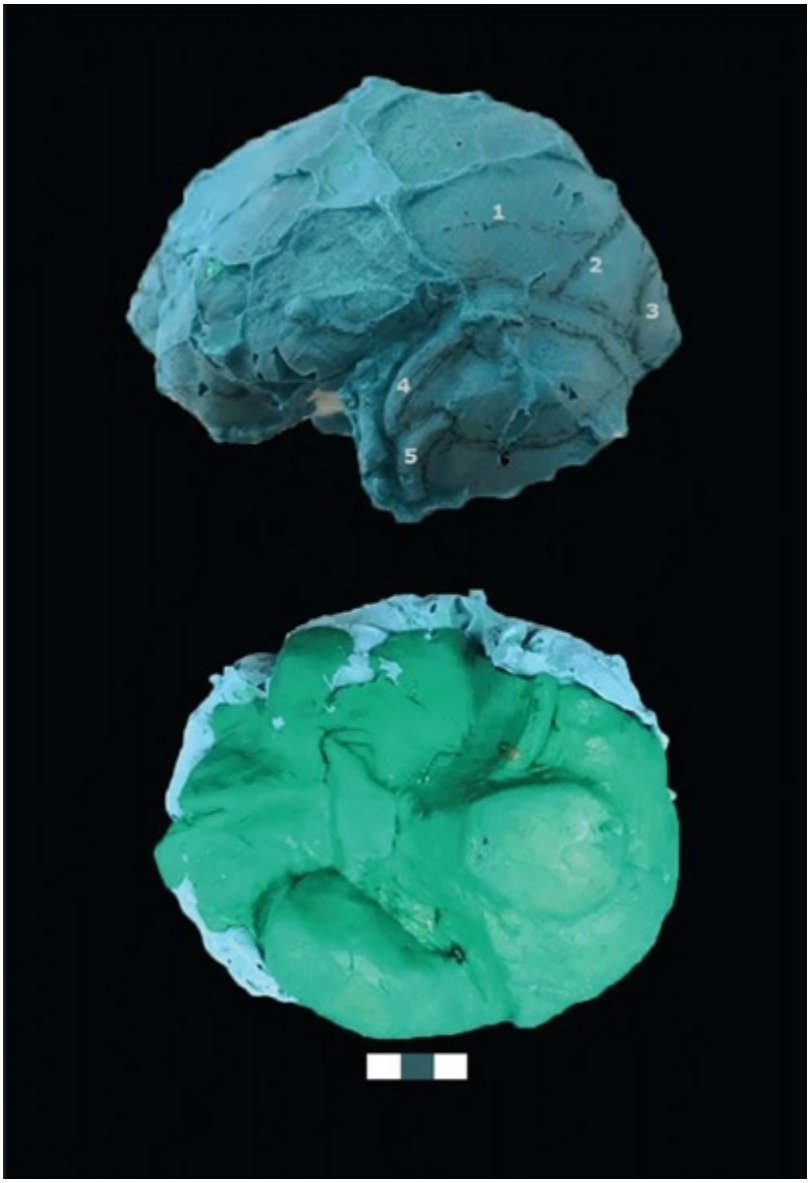

Supplementary Figure S3.
LES1 silicone endocast physical model in left lateral (top) and basal (bottom) views. This model uses comparative data to build the basicranial anatomy. The measured volume of this reconstruction is 590cc, smaller than the digital reconstruction which had a volume of 610cc (Holloway et al., 2018). 1, Meningeal vessel; 2, lambdoid suture; 3, small sulcus of occipital lobe and pole; 4, sigmoid sinus; 5, interior portion of sigmoid sinus, displaced; 6, greater cerebellar horizontal sulcus.

106x155mm (96 x 96 DPI)

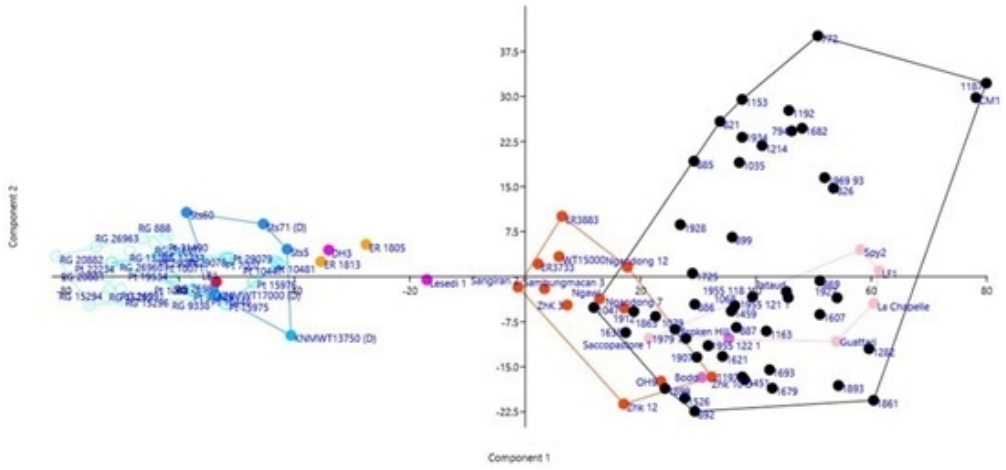

Supplementary Figure S4.
Results of principal components analysis (PCA) based on interlandmark distances. PC1 accounts for 86.4% of the variance and has positive weights on all underlying interlandmark distances. The rank order of fossil hominins on this axis is basically in order of endocranial volume. PC2 accounts for 5.9% of the variance and appears to show a degree of within-group variation in each sample.

144x67mm (96 x 96 DPI)

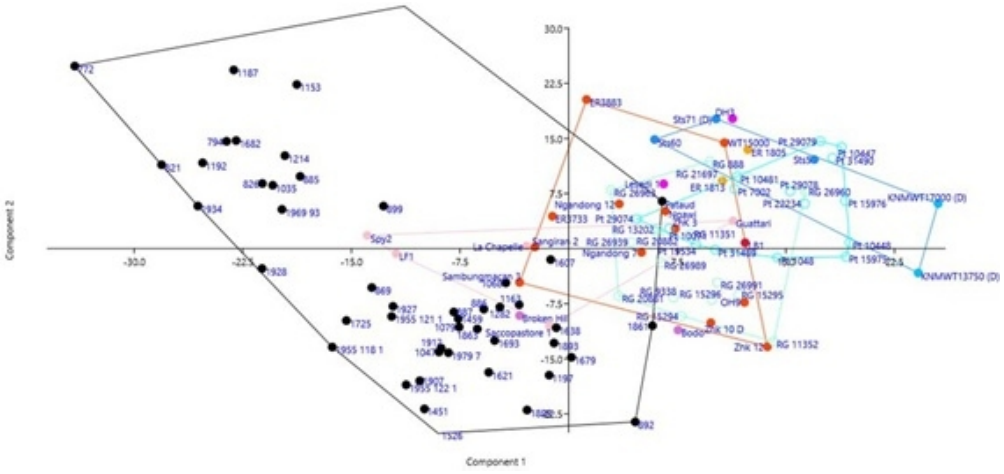

Supplementary Figure S5.
Results of principal components analysis (PCA) based on interlandmark distances relative to cube root endocranial volume. In this analysis, PC1 still appears correlated with endocranial size, although with length relative to height reflected in this dimension.

150x70mm (96 x 96 DPI)

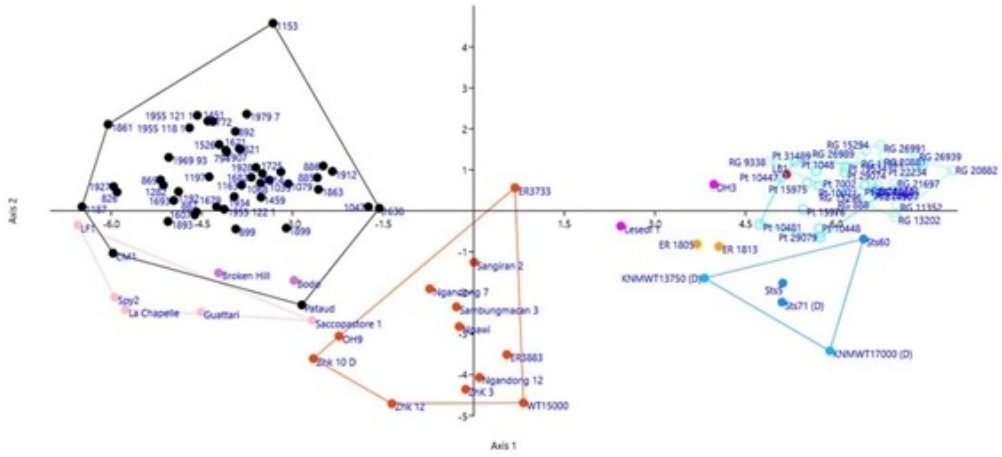

Supplementary Figure S6.
Results of linear discriminant analysis (LDA) based on absolute interlandmark distances. These results are also reported in main text Figure 2, here provided with all fossil hominin individuals labeled. Axis 1 is strongly correlated with endocranial volume, while axis 2 separates samples based on dimensions associated with endocast length relative to height. H. naledi in this analysis is well discriminated from other samples of similar endocranial volume, including H. habilis, Australopithecus-Paranthropus, and H. erectus.

148x67mm (96 x 96 DPI)

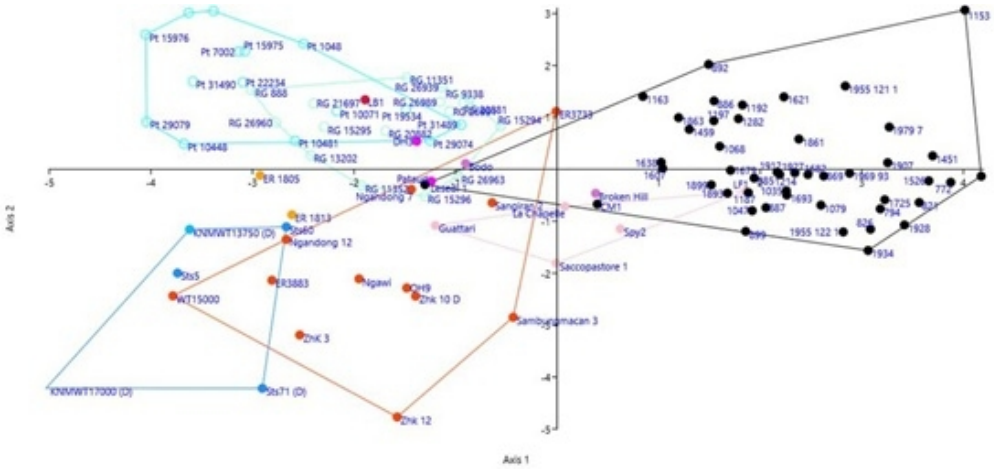

Supplementary Figure S7.
Results of linear discriminant analysis (LDA) based on interlandmark distances relative to cube root endocranial volume. These results are also reported in main text Figure 2, here provided with all fossil hominin individuals labeled.

144x67mm (96 x 96 DPI)

		HF3	LF3	SF3	HF3r	LF3r
H. naledi	mean	6.5	36.8	120.6	8	45.5
	N	2	2	2	2	2
	V*	17.5	13.6	30.8	10.8	6.9
H. sapiens	mean	5.6	36.7	105.7	5	32.4
	N	139	139	139	139	139
	V*	26.1	12	34.2	26.2	12.8
P. paniscus	mean	2.4	23.6	29.1	3.5	33.6
	N	35	35	35	35	35
	V*	20.7	9.2	24.3	20.7	8.5
P. troglodytes	mean	2.9	22	32.2	4	30.2
	N	36	36	36	36	36
	V*	25	9.3	30.3	26	9.2
H. erectus	mean	6.4	34.7	111.3	6.6	35.7
	N	12	12	12	12	12
	V*	26.7	20.1	41	26.1	13.7
H. neanderthalensis	mean	7.5	35.2	167.7	6.7	31.2
	N	11	11	11	11	11
	V*	27.9	34	19.9	26	32.1

		PF -B	PF -C	PF -W	PF- TC	B- TP	B- W	B- C
	me	**38**	**79**	**94**	**104**	**19**	**62**	**76**
H. naledi	**an**	**6**	**2**	**5**	**0.7**	**5**	**0.9**	**8**
	N	2	2	2	2	2	2	2
	V*	14 4	10 1	7.2	4.9	8.8	4 3	9.9
	me	**50**	**11**	**11**	**123**	**24**	**71**	**10**
H. sapiens	**an**	**5**	**0.1**	**3.3**	**0**	**6**	**0.8**	**7**
	N	45	45	45	45	45	45	45
	V*	7	6.4	6.9	5	25 2	15 0.5	5.9
	me	**34**	**68**	**72**	**86**	**20**	**41**	**63**
P. paniscus	**an**	**9**	**2**	**6**	**7**	**5**	**0.7**	**8**
	N	16	16	16	16	16	16	16
	V*	8.7	6.7	5.6	4.8	13 4	12 0.8	6
P.	**me**	**38**	**76**	**77**	**93**	**21**	**43**	**70**
troglodytes	**an**	**6**	**0**	**4**	**0**	**8**	**0.3**	**5**
	N	15	15	15	15	15	15	15
	V*	7.3	6.2	7.4	5	12 7	12 0.1	5.3
	me	**50**	**10**	**10**	**119**	**28**	**62**	**91**
H. erectus	**an**	**9**	**3.8**	**7.5**	**0.9**	**2**	**0.4**	**3**
	N	12	12	12	12	12	12	12
	V*	11 6	7.1	4.5	4.4	14 7	11 0.3	6.4
H.								
neanderthal	**me**	**54**	**11**	**12**	**131**	**31**	**75**	**10**
ensis	**an**	**8**	**2**	**3.3**	**0.5**	**1**	**0.5**	**4.1**
	N	7	6	7	6	6	7	6
	V*	6.5	6.6	6.1	5.9	15 4	10 0.2	7.7
	me	**43**	**80**	**92**	**108**	**19**	**56**	**72**
H. habilis	**an**	**1**	**7**	**9**	**0.8**	**1**	**0**	**1**
	N	3	2	3	2	2	3	2
	V*	3.3	0	5.9	5.1	18 7	18 0	0.3
Au.	**me**	**40**	**76**	**82**	**99**	**23**	**47**	**64**
africanus	**an**	**8**	**1**	**9**	**5**	**8**	**0.1**	**3**
	N	3	3	3	3	3	3	3
	V*	13 7	7.7	1.5	5.9	14 0	10 0.2	4.7
Paranthrop	**me**	**45**	**72**	**82**	**104**	**20**	**46**	**66**
us	**an**	**6**	**1**	**6**	**0.4**	**8**	**0.2**	**2**
	N	2	2	3	3	3	3	3
			10				24	11

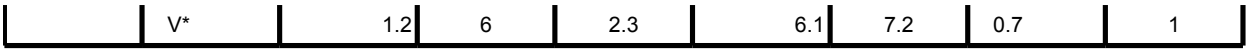
V*
1.2
6
2.3
6.1
7.2
0.7
1

TP- TC	TC -C	W- TC	W -C	W -E	C- O	TC -O	E- O	W -O
67	**81**	**19**	**74**	**65**	**87**	**46**	**18**	**62**
3	**8**	**4**	**0.8**	**0**	**7**	**8**	**0**	**0.8**
2	3	4	3	2	1	2	2	2
		15	4	0			14	6
4.4	3.6	9	9	0		2.3	0.3	0
73	**11**	**37**	**92**	**91**	**10**	**75**	**26**	**90**
9	**1.3**	**4**	**0.3**	**0.9**	**7.3**	**2**	**0.1**	**0.5**
45	45	45	45	45	45	45	45	45
		31	10	6			15	6
7.9	5.2	6	0.9	4	6.2	8.4	0	4
54	**66**	**20**	**60**	**59**	**63**	**39**	**14**	**55**
4	**1**	**6**	**0.9**	**0.4**	**0**	**9**	**0.8**	**0.7**
16	16	16	16	16	16	16	16	16
		21	5	6			14	8
7.2	4.9	9	6	5	6.6	7.4	0.6	7
59	**66**	**23**	**63**	**62**	**57**	**41**	**13**	**58**
3	**5**	**0**	**0.7**	**0.2**	**7**	**6**	**0.8**	**0.5**
15	15	15	15	14	14	14	14	14
		17	5	5		10	14	8
7.4	5.7	4	7	0	9.6	3	0	4
70	**93**	**24**	**84**	**79**	**92**	**61**	**26**	**77**
5	**4**	**8**	**0.9**	**0.7**	**9**	**5**	**0.6**	**0.8**
12	12	13	12	13	12	13	13	13
		14	9	9		13	17	14
7.5	7	4	3	0	6.8	5	0.6	0.1
74	**11**	**30**	**98**	**86**	**10**	**76**	**32**	**88**
9	**2.9**	**5**	**0.8**	**0.6**	**7.7**	**0**	**0.2**	**0.3**
6	6	7	7	6	7	6	6	7
13		18	3	3			11	5
2	5.6	2	7	7	3.7	4.8	0.9	9
65	**81**	**28**	**69**	**67**	**79**	**38**	**20**	**57**
5	**9**	**3**	**0.8**	**0.9**	**8**	**1**	**0.3**	**0.6**
2	3	3	3	3	3	3	3	4
		11	10	8			18	8
8.6	5.2	0	0	4	5.3	1.4	0.5	1
62	**75**	**28**	**58**	**61**	**72**	**35**	**17**	**54**
1	**0**	**4**	**0.7**	**0.6**	**5**	**9**	**0.5**	**0.2**
3	3	3	3	3	3	3	3	3
		14	5	12		12	23	16
7	7.6	7	5	0.3	5.7	1	0.1	0.1
63	**74**	**25**	**70**	**67**	**74**	**44**	**18**	**64**
8	**2**	**4**	**0.1**	**0.5**	**2**	**3**	**0.6**	**0.2**
3	4	5	4	5	4	5	5	5
		31	11	16		11	20	16

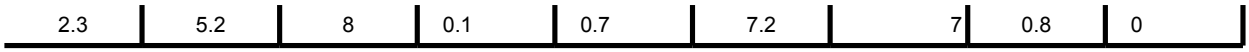
2.3
5.2
8
0.1
0.7
7.2
7
0.8
0

		PF-Br	PF-Cr	PF-Wr	PF-TCr	B-TPr	B-Wr	B-Cr
H. naledi	**mean**	**47.5**	**97.5**	**116.5**	**129.1**	**24.2**	**77.6**	**94.6**
	N	2	2	2	2	2	2	2
	V*	7.2	2.9	0	2.3	15.9	2.9	2.7
H. sapiens	**mean**	**45.4**	**98.9**	**101.8**	**110.6**	**22.1**	**64.5**	**96.1**
	N	45	45	45	45	45	45	45
	V*	6.4	5.3	5.8	3.7	24.3	14.7	4.3
P. paniscus	**mean**	**49.4**	**96.6**	**102.8**	**122.7**	**29.1**	**59.0**	**90.3**
	N	16	16	16	16	16	16	16
	V*	9.3	6.8	5.1	3	12.2	12.3	5.8
P. troglodytes	**mean**	**53.1**	**104.5**	**106.2**	**127.9**	**29.9**	**59.5**	**96.9**
	N	15	15	15	15	15	15	15
	V*	4.6	6.7	4.6	2.8	12.6	10.4	5.3
H. erectus	**mean**	**51.6**	**105.3**	**109.3**	**121.7**	**28.7**	**63.6**	**92.7**
	N	12	12	12	12	12	12	12
	V*	7.7	4	5.5	2.9	14.9	14.5	5.2
H. neanderthalensis	**mean**	**48.4**	**98.0**	**108.9**	**116.5**	**27.6**	**66.5**	**91.1**
	N	7	6	7	6	6	7	6
	V*	7.2	3.2	2.8	5.3	16.1	6.5	4.7
H. habilis	**mean**	**51.9**	**98.9**	**111.7**	**133.2**	**23.3**	**67.1**	**88.3**
	N	3	2	3	2	2	3	2
	V*	7.1	3.6	2.8	1.5	15.2	14.4	3.3
Au. africanus	**mean**	**53.6**	**100.3**	**109.3**	**131.0**	**31.4**	**62.2**	**84.7**
	N	3	3	3	3	3	3	3
	V*	10.3	5	2.8	2.4	13.0	13.2	1.2
Paranthropus	**mean**	**59.9**	**94.6**	**106.5**	**134.6**	**26.8**	**59.2**	**85.0**
	N	2	2	3	3	3	3	3

	V*	2.7	6.7	2.7	3.5	11 0	21 0	7 4

TP-TCr	TC-Cr	W-TCr	W-Cr	W-Er	C-Or	TC-Or	E-Or	W-Or
83	**100**	**24**	**91**	**81**	**106**	**58**	**22**	**78**
2	**0.3**	**2**	**8**	**3**	**0.4**	**7**	**0.5**	**8**
2	3	4	3	2	1	2	2	2
11.6	3	20 2	1.9	5		7.3	9 4	10 9
66	**100**	**33**	**83**	**82**	**96**	**67**	**23**	**81**
5	**0**	**5**	**0**	**6**	**4**	**6**	**0.4**	**3**
45	45	45	45	45	45	45	45	45
7.5	3.9	31 0	10 8	5.3	5.5	7.9	14 0.6	6
77	**93**	**29**	**86**	**84**	**89**	**56**	**20**	**78**
0	**5**	**0**	**2**	**1**	**1**	**5**	**0.9**	**9**
16	16	16	16	16	16	16	16	16
5.8	3.4	20 6	4.7	5.1	5.3	8.5	12 0.4	8.3
81	**91**	**31**	**87**	**84**	**78**	**56**	**18**	**79**
5	**4**	**7**	**5**	**8**	**8**	**7**	**0.8**	**8**
15	15	15	15	14	14	14	14	14
5.8	4.4	19 0	4.3	4.5	9	9.5	15 0	7.6
71	**94**	**25**	**86**	**81**	**94**	**62**	**27**	**79**
6	**9**	**4**	**2**	**4**	**3**	**7**	**0.2**	**3**
12	12	13	12	13	12	13	13	13
5.7	5.3	14 0	7.3	5.3	3.9	9.9	16 0.5	10 0
66	**99**	**27**	**86**	**76**	**94**	**66**	**28**	**77**
3	**3**	**0**	**8**	**2**	**5**	**8**	**0.4**	**6**
6	6	7	7	6	7	6	6	7
12.8	3.7	15 5	4.6	3.9	2.9	4	13 0.1	7.5
80	**98**	**33**	**83**	**81**	**95**	**45**	**24**	**68**
1	**3**	**9**	**7**	**5**	**8**	**8**	**0.4**	**6**
2	3	3	3	3	3	3	3	4
5.1	0.8	9.2	6.5	8.8	3.5	3	18 0.1	8.3
81	**98**	**37**	**77**	**81**	**95**	**47**	**23**	**71**
7	**8**	**4**	**4**	**1**	**6**	**3**	**0.1**	**3**
3	3	3	3	3	3	3	3	3
3.6	5.6	11 1	3.2	10 1	3.3	12 0	22 0.3	14 1
82	**96**	**32**	**90**	**86**	**96**	**57**	**24**	**82**
2	**1**	**6**	**9**	**8**	**2**	**1**	**0**	**6**
3	4	5	4	5	4	5	5	5

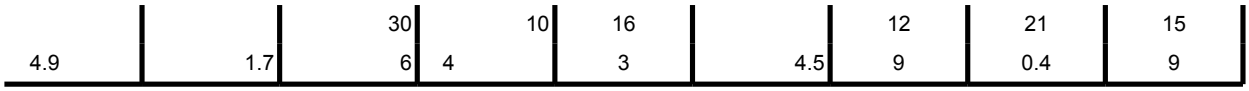
30
10
16
12
21
15
4.9
1.7
6
4
3
4.5
9
0.4
9

	PF-B	PF-C	PF-W	PF-TC	B-PT	B-W	B-C	PT-TC
Lesedi 1	**42.1**	**84.2**	**98.8**	**108**	**18.5**	**64.6**	**81.6**	**65.4**
Azs *H. sapien*	-1.2	-1.8	-0.9	-1.2	-0.5	-0.3	-2	-0.7
Azs *Pan panis*	1.1	1.6	3	2.3	-0.4	2	2.2	1.3
Azs *Pan troglo*	0.3	0.5	1.6	1.3	-0.2	2	1	1.1
Azs *H. erectus*	-0.7	-1.2	-0.8	-1	-1.1	0.1	-0.7	-0.4
Azs *H. neande*	-1.6	-1.6	-1.3	-1.2	-0.8	-0.5	-1.2	-0.2
DH3	**35.1**	**74.1**	**90.2**	**102**	**20.6**	**61.3**	**72**	**69.2**
Azs *H. sapien*	-2.1	-2.5	-1.5	-1.7	-0.3	-0.5	-2.7	-0.4
Azs *Pan panis*	0	0.6	2	1.6	0	1.7	1	1.8
Azs *Pan troglo*	0.3	0.5	1.6	1.3	-0.2	2	1	1.1
Azs *H. erectus*	-1.2	-1.8	-1.6	-1.5	-0.8	-0.1	-1.5	-0.1
Azs *H. neande*	-1.6	-1.6	-1.3	-1.2	-0.8	-0.5	-1.2	-0.2
DH1								
Azs *H. sapiens*								
Azs *Pan paniscus*								
Azs *Pan troglodytes*								
Azs *H. erectus*								
Azs *H. neanderthalensis*								
DH4								
Azs *H. sapiens*								
Azs *Pan paniscus*								
Azs *Pan troglodytes*								
Azs *H. erectus*								
Azs *H. neanderthalensis*								

TC-C	W-TC	W-C	W-E	C-O	TC-O	E-O	W-O
82.4	**16.2**	**76.6**					
-2.5	-0.9	-0.8					
2.3	-0.5	2.1					
1.6	-0.5	1.3					
-0.8	-1.1	-0.5					
-2	-0.9	-2.7					
78.8	**20.1**	**71**					
-2.8	-0.7	-1.1					
1.8	0	1.4					
1.6	-0.5	1.3					
-1	-0.6	-0.8					
-2	-0.9	-2.7					
84.1	**18.3**	**77**	**64.9**	**87.7**	**46.1**	**19.6**	**60.5**
-2.3	-0.8	-0.8	-2.3	-1.5	-2.3	-0.8	-2.5
2.6	-0.2	2.2	0.7	2.7	1	1	0.5
1.6	-0.5	1.3	0.4	2.5	0.5	1.4	0.2
-0.6	-0.8	-0.4	-0.9	-0.4	-0.8	-0.7	-0.7
-2	-0.9	-2.7	-2.6	-2	-3	-1.2	-2.1
	23		**65**		**47.5**	**16.4**	**65.2**
	-0.6		-2.3		-2.2	-1.2	-2.1
	0.3		0.7		1.2	0.3	0.9
	-0.5		0.4		0.6	0.6	0.6
	-0.2		-0.9		-0.8	-1	-0.5
	-0.9		-2.6		-2.9	-1.5	-1.8

	PF-Br	PF-Cr	PF-Wr	PF-TCr	B-PTr	B-Wr	B-Cr	PT-TCr
Lesedi 1	**50**	**99**	**117**	**127**	**22**	**76**	**96**	**77**
Azs *H. sapie*	0.7	0	1.2	2	0	0.6	0	1.1
Azs *Pan pa*	0	0.2	1.2	0.6	-1	1.1	0.5	0
Azs *Pan tro*	-1	0	1	0	-1	1.2	0	0
Azs *H. erec*	0	-1	0.5	0.7	-1	0.6	0.3	0.6
Azs *H. near*	0.1	0.1	1	0.6	-1	0.9	0.5	0.5
DH3	**45**	**96**	**117**	**131**	**27**	**79**	**93**	**89**
Azs *H. sapie*	0	0	1.2	2.4	0.4	0.8	0	2.3
Azs *Pan pa*	0	0	1.2	1	0	1.3	0.2	1.3
Azs *Pan tro*	-2	-1	1	0.4	0	1.5	0	0.8
Azs *H. erec*	-1	-1	0.5	1.2	0	0.7	0	1.9
Azs *H. near*	0	0	1	0.9	0	1.1	0.2	1
DH1								
Azs *H. sapiens*								
Azs *Pan paniscus*								
Azs *Pan troglodytes*								
Azs *H. erectus*								
Azs *H. neanderthalensis*								
DH4								
Azs *H. sapiens*								
Azs *Pan paniscus*								
Azs *Pan troglodytes*								
Azs *H. erectus*								
Azs *H. neanderthalensis*								

TC-Cr	W-TCr	W-Cr	W-Er	C-Or
97	**19**	**90**		
0	-1	0.4		
0.5	-1	0.5		
0.6	-1	0.3		
0.2	-1	0.3		
0	-1	0.3		
102	**26**	**92**		
0.2	0	0.5		
1.2	0	0.6		
1.2	0	0.5		
0.6	0.1	0.4		
0.2	0	0.5		
102	**22**	**93**	**79**	**106**
0.3	-1	0.6	0	0.9
1.3	-1	0.8	-1	1.7
1.2	-1	0.7	-1	1.8
0.6	0	0.5	0	1.5
0.3	-1	0.7	0.3	1.7
	30		**84**	
	0		0.1	
	0.1		0	
	0		0	
	0.5		0.3	
	0.3		1	